JASS Journal of Astronomy and Space Sciences

# A Study of Double Dark Photons Produced by Lepton Colliders using High Performance Computing

**Kihong Park[1,2], Kyungho Kim[2], Kihyeon Cho[1,2†]**

[1]University of Science and Technology, Daejeon 34113, Korea
[2]Korea Institute of Science and Technology Information, Daejeon 34141, Korea

The universe is thought to be filled with not only Standard Model (SM) matters but also dark matters. Dark matter is thought to play a major role in its construction. However, the identity of dark matter is as yet unknown, with various search methods from astrophysical observartion to particle collider experiments. Because of the cross-section that is a thousand times smaller than SM particles, dark matter research requires a large amount of data processing. Therefore, optimization and parallelization in High Performance Computing is required. Dark matter in hypothetical hidden sector is though to be connected to dark photons which carries forces similar to photons in electromagnetism. In the recent analysis, it was studied using the decays of a dark photon at collider experiments. Based on this, we studies double dark photon decays at lepton colliders. The signal channels are $e^+e^- \rightarrow A'A'$ and $e^+e^- \rightarrow A'A'\gamma$ where dark photon $A'$ decays dimuon. These signal channels are based on the theory that dark photons only decay into heavily charged leptons, which can explain the muon magnetic momentum anomaly. We scanned the cross-section according to the dark photon mass in experiments. MadGraph5 was used to generate events based on a simplified model. Additionally, to get the maximum expected number of events for the double dark photon channel, the detector efficiency for several center of mass (CM) energy were studied using Delphes and MadAnalysis5 for performance comparison. The results of this study will contribute to the search for double dark photon channels at lepton colliders.

**Keywords:** astrophysics, dark matter, dark photon, lepton collider, high performance computing

## 1. INTRODUCTION

Astronomical observations have shown that our universe is filled with not only Standard Model (SM) matters but also dark matters. It accounts for most of the substances that make up the universe, but has not yet been detected directly or indirectly (Cho 2016a, b). Given the interaction of SM particles, it is natural to assume the interaction of dark sector materials. Dark photons mediate the interaction between the dark matter and SM particles. Dark matter has little effect on everyday experiments. However, it makes fundamental changes to the movement of celestial bodies and the evolution of the universe via macroscopic gravity-related phenomena. Since it was revealed that dark matter cannot be explained by known physics in SM,

theoretical and experimental studies have been conducted to find candidate substances for dark matter. To identify dark matter, it is necessary to integrate and analyze "big data" obtained from various experiments and compare it to simulations derived from theory. Therefore, research has been conducted on the convergence of experiments, theory, and simulation using high-performance computing (HPC; Cho 2016a, b; Cho 2017; Yeo & Cho 2018). As dark matter has a small cross-section, a large amount of simulation data must be generated (Cho 2017). Therefore, efficient research on HPC is required (Choi et al. 2018; Yeo & Cho 2019; Yeo & Cho 2020). Previously, we had studied it using $e^+e^- \rightarrow \mu^+\mu^-A'$ mode (Park & Cho 2021a, b). Based on this information (Yeo & Cho 2018; Park & Cho 2021a, b), we also studied double dark photons produced by lepton colliders. Using the simplified

model, we studied $e^+e^- \to A'A'$ where each $A'$ decays into dimuon (Alves et al. 2012). Similar to initial state radiation (ISR) gluon generation in hadron colliders, ISR photons are generated in lepton colliders. As ISR photons affect the cross-section, we also studied the decay of $e^+e^- \to A'A'\gamma$ where each $A'$ decays into dimuon. This decay includes the ISR photon.

## 2. METHODS

Based on the previous study on CPU time consumed for simulation (Park & Cho 2021a, b), we effectively used the KISTI-5 supercomputer (Nurion Knights Landing and Skylake) for HPC. Fig. 1 shows the flow chart of the study. To obtain physical properties, a physics simulation was performed using MadGraph5 (Alwall et al. 2014; MadGraph5, 2022) on the KISTI-5 supercomputer. We generated current and future lepton colliders events for center of mass (CM) energies between 1 and 3,000 GeV. Table 1 shows the current and future lepton collider experiments (Zyla et al. 2020). First, event generation was performed using the KISTI-5 supercomputer. Detector simulation, reconstruction, and fitting were performed using a local Linux machine. Feynman diagrams were generated using simplified model (Alves et al. 2012). To obtain detector efficiency, we performed a full simulation at the energies of lepton collider experiments. We used Delphes for detector simulation
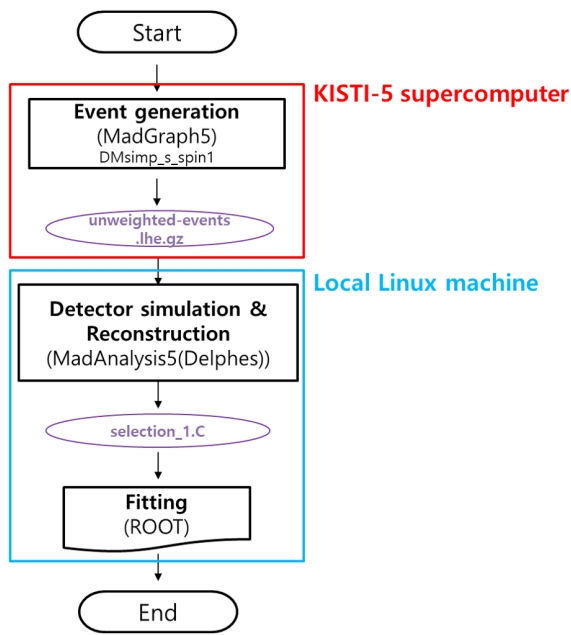


**Fig. 1.** The flow chart of the study.

**Table 1.** Parameters of current and future lepton colldier experiments

| Experiments | Type | CM energy (GeV) | Circumference / length (km) |
|---|---|---|---|
| Belle II | Circular | 10.58 ($e^-$: 7, $e^+$: 4) | 3.0116 |
| FCC-ee (Future circular collider) | Circular | 92 240 366 | 97.75 |
| CEPC (Circular electron positron collider) | Circular | 92 240 | 100 |
| ILC (International linear collider) | Linear | 250 500 | 20.5 31 |
| CLIC (Compact linear collider) | Linear | 380 3,000 | 11 50 |

Adapted from Zyla et al. (2020) with public domain.
FCC-ee, future circular collider.

(Favereau et al. 2014; Delphes 2022). We used MadAnalysis5 for reconstruction (Conte et al. 2013; MadAnalysis5 2022). We used ROOT (Antcheva et al. 2009; ROOT 2022) to plot and fit the data.

## 3. THEORY

Dark matter rarely interact with SM particles, but interactions can occur using dark photons as a portal. Dark sectors can be classified according to the interaction mechanism between dark matter and SM particles. Dark photons can only interact with heavily charged leptons such as muons and taus, and their sector is called the type 4 dark sector (Shuve & Yavin 2014; Yeo & Cho 2018). One advantage of the type 4 dark sector is that it can explain the anomaly of the muon's magnetic momentum (Shuve & Yavin 2014). In this study, we have investigated dark matter through channels where dark photon decays into dimuon in lepton collider experiments. The signal modes are $e^+e^- \to A'A'$ and $e^+e^- \to A'A'\gamma$ where each $A'$ decays into dimuon. As this model includes SM particles, and dark sector particles the coupling constant between SM particles and dark photons can be implemented. In particular, the ISR plugin in MadGraph5 was used to study the ISR effect on cross-sections. To study the background event, four muon final states (the same final state particle as the signal event) were selected from the SM. The signal cross-section depends on the CM energy. It also depends on dark photon mass and coupling constant. Therefore investigating the cross-section according to each parameter is important for successful signal event acquisition from particle collider experiments. Therefore, we studied the parameter effects on the cross-section for not only signal events but also background events. We used the KISTI-5 supercomputer to accommodate the large amount of computation and memory required to produce the broad

parameter space for event generation.

# 4. DOUBLE DARK PHOTON GENERATION

## 4.1. Cross-Section of Background Processes, $e^+e^- \rightarrow \mu^+\mu^-\mu^+\mu^-(\gamma)$

The background processes were $e^+e^- \rightarrow \mu^+\mu^-\mu^+\mu^-$ and $e^+e^- \rightarrow \mu^+\mu^-\mu^+\mu^-\gamma$ based on the SM. Table 2 lists parameters of the SM background. The KISTI-5 supercomputer was utilized for background event generation. The events were generated using MadGraph5 (version 2.6.6), as ISR plug-in is available and has been verified in this version. The minimum transverse momentum ($P_T$) cuts for photons and leptons are

set to 0.01 in order to generate events at energies less than 40 GeV. In total, 10,000 events were generated. The range of CM energy was chosen from 1 GeV to 3,000 GeV.

For the event $e^+e^- \rightarrow \mu^+\mu^-\mu^+\mu^-$, there are total 48 Feynman diagrams. Among them, only four modes are dominant as shown in Fig. 2. The γ interaction mode and the γ-γ interaction mode are the only photon-involved modes that contribute to the cross-section throughout the energy range. The Z interaction mode and the Z-γ interaction mode are responsible for the peak occurring near 91 GeV due to a Z-boson interaction. Fig. 3 shows the cross-section of the SM backgournd of $e^+e^- \rightarrow \mu^+\mu^-\mu^+\mu^-$ depending on CM energy. A peak occurrs at 90 GeV due to the Z-boson interaction.

For the event $e^+e^- \rightarrow \mu^+\mu^-\mu^+\mu^-\gamma$, there are total 336

**Table 2.** Parameters of SM background

| Specification | $e^+e^- \rightarrow \mu^+\mu^-\mu^+\mu^-$ | $e^+e^- \rightarrow \mu^+\mu^-\mu^+\mu^-\gamma$ |
|---|---|---|
| Machine | KISTI-5 supercomputer | |
| Simulation tool kit | MadGraph5 v2.6.6 | |
| Importing model | The standard model (default) | |
| Command | generate e+ e- > mu+ mu- mu+ mu- | generate e+ e- > mu+ mu- mu+ mu- a |
| Condition | $P_{T,\mu} \geq 0.01$ GeV, $P_{T,\gamma} \geq 0.01$ GeV | |
| Number of generated events | 10,000 | |
| CM energy [GeV] | 1, 2, ..., 9, 10, 20, ..., 490, 500, 600, 700, ..., 2,900, 3,000 | |

SM, standard model; KISTI, Korea Institute of Science and Technology Information.
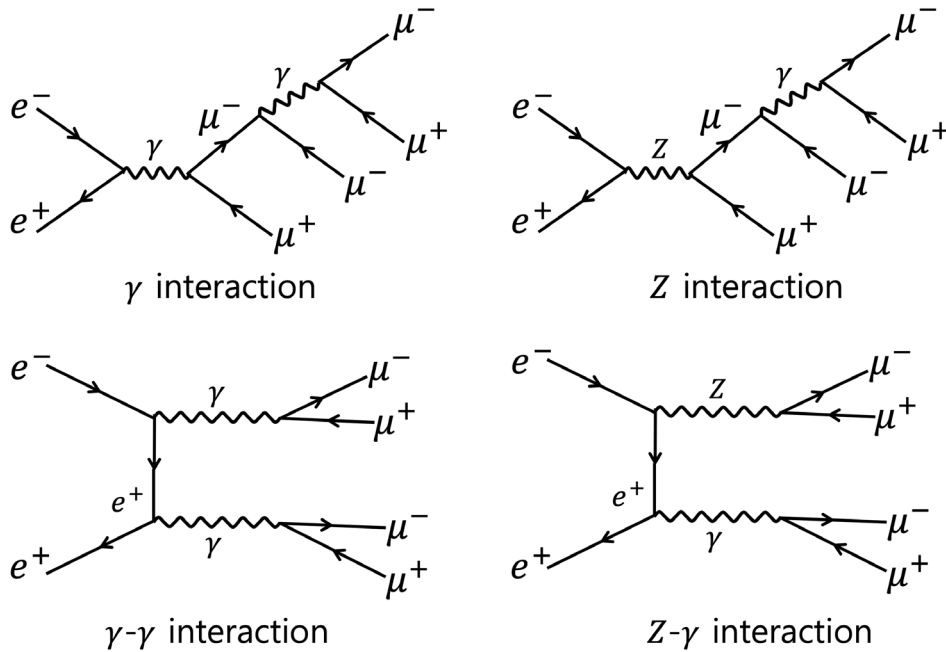


**Fig. 2.** The dominant Feynman diagrams of the $e^+e^- \rightarrow \mu^+\mu^-\mu^+\mu^-$.

Feynman diagrams. Among them, only four modes are dominant as shown in Fig. 4. The Z interaction with the ISR γ mode contributes to the peak near 90 GeV via Z-boson interaction. The Z-Z interaction with the ISR γ mode is a process accompanying the ISR and contributes to the entire scanned energy range. The Z-Z interaction contributes to the peak occurring at approximately 180 GeV through two Z-boson interactions. Fig. 5 shows the cross-section depending on CM energy for the SM background of $e^+e^- \to \mu^+\mu^-\mu^+\mu^-\gamma$.
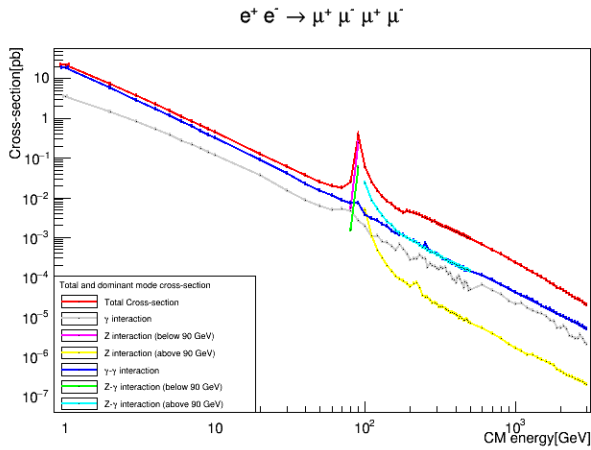


**Fig. 3.** The cross-section of SM background of $e^+e^- \to \mu^+\mu^-\mu^+\mu^-$ dependening on CM energy. SM, standard model.
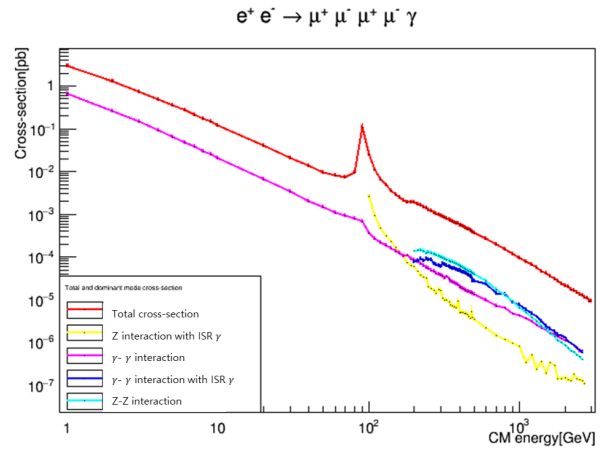


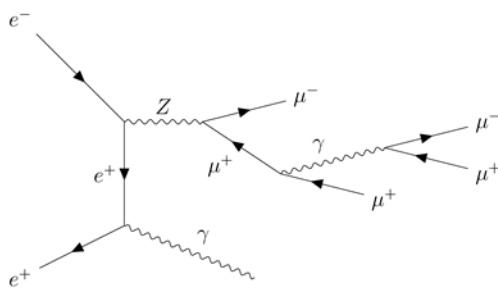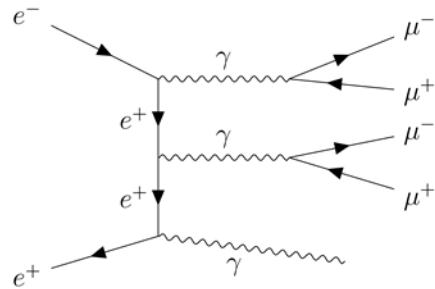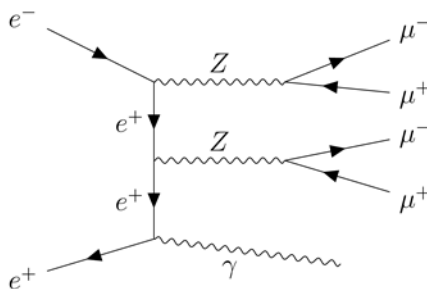**Fig. 5.** The cross-section depending on CM energy of SM background of $e^+e^- \to \mu^+\mu^-\mu^+\mu^-\gamma$. SM, standard model.



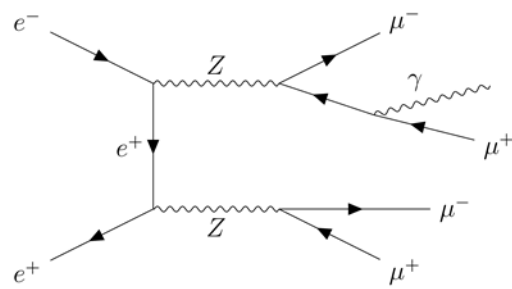**Fig. 4.** The dominant Feynman diagrams of the $e^+e^- \to \mu^+\mu^-\mu^+\mu^-\gamma$.

### 4.2 Cross-Section of Signal Processes , $e^+e^- \rightarrow A'A'(\gamma)$

The signal processes are $e^+e^- \rightarrow A'A'$ and $e^+e^- \rightarrow A'A'\gamma$ where each $A'$ decays into dimuon. Fig. 6 shows the Feynman diagrams of the signal process, with four coupling constants indicated by red circles. Three physical parameters were involved in the signal processes, the CM energy, dark photon mass, and coupling constant. Therefore, we studied the cross-section according to each physical parameter. Table 3 summarizes the coupling constants. A and C are the coupling constants of the electrons and dark photons respectively, and B and D are those for the muons and dark photons respectively. These values were changed to scan the coupling constants.

Detailed information for generating the signal event is summarized in Table 4. We used the KISTI-5 supercomputer to generate signal events. The minimum transverse momentum ($P_T$) cut for photons and leptons was set at 0.01, which was the same as for background event generation. Fig. 7 shows the dominant Feynman diagram for $e^+e^- \rightarrow A'A'$ where each
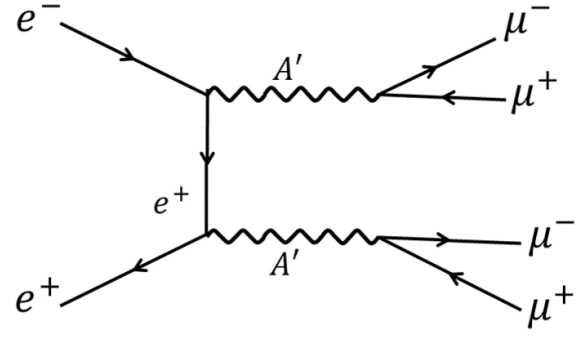


**Fig. 7.** The signal dominant Feynman diagram of $e^+e^- \rightarrow A'A'$ where each $A'$ decays into dimuon.

$A'$ decays into dimuon. Fig. 8 shows the dominant Feynman diagrams of $e^+e^- \rightarrow A'A'\gamma$ where each $A'$ decays into dimuon.

#### 4.2.1 Cross-Section Depending on CM Energy

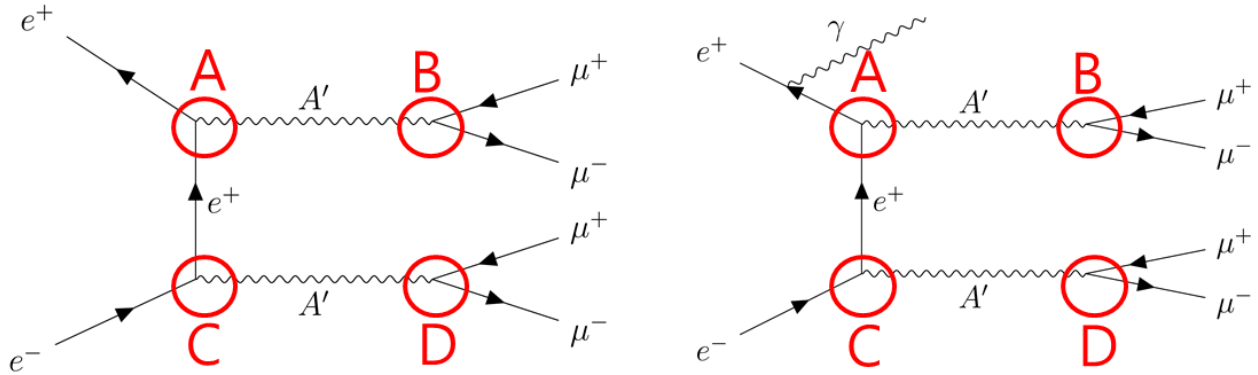The CM energy was scanned for the cross-section of the



**Fig. 6.** Feynman diagrams of signal processes illustrating the coupling constants (left: without ISR γ, right: with ISR γ). ISR, initial state radiation.

**Table 3.** The summary of the coupling constants

|       | Theory | MadGraph5 | Default value | Description |
|-------|--------|-----------|---------------|-------------|
| A, C  | $g^v_{l_{11}}$ | gvl11 | 1 | Electron-Y1 vector coupling |
| B, D  | $g^v_{l_{22}}$ | gvl22 | 1 | Muon-Y1 vector coupling |

**Table 4.** Parameters of dark photon signal

| Specification | $e^+e^- \rightarrow A'A'$ | $e^+e^- \rightarrow A'A'\gamma$ |
|---------------|--------------------------|----------------------------------|
| Machine | KISTI-5 supercomputer | |
| Simulation tool kit | MadGraph5 v2.6.6 | |
| Imported model | Simplified model | |
| Command | generate e+ e– > y1 y1 , y1 > mu+ mu- | generate e+ e– > y1 y1 a, y1 > mu+ mu- |
| Condition | $P_{T,\mu} \geq 0.01$ GeV, $P_{T,\gamma} \geq 0.01$ GeV | |
| Number of generated events | 10,000 | |

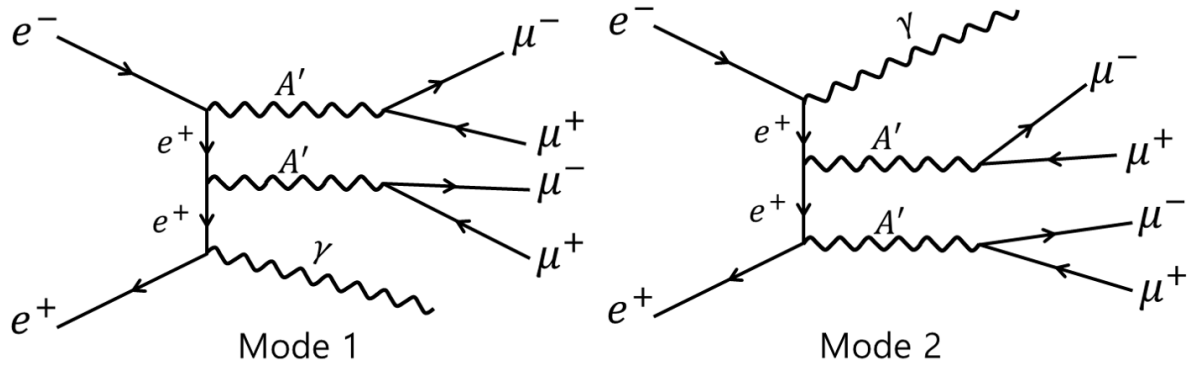KISTI, Korea Institute of Science and Technology Information.

**Fig. 8.** The dominant Feynman diagrams of $e^+e^- \rightarrow A'A'\gamma$ where each $A'$ decays into dimuon.

signal process between 1 and 3,000 GeV. The dark photon mass was set as 0.3 GeV (greater than the dimuon mass). The dark photon width was fixed at $6.7 \times 10^{-6}$ GeV. The coupling constant was fixed at 0.1. The minimum transverse momentum ($P_T$) cut for photons and leptons was set at 0.01. Fig. 9 shows that the cross-section decreases as the CM energy increases for the signal process $e^+e^- \rightarrow A'A'$. After applying the ISR plugin, the cross-section increased slightly, due to the actual CM energy being slightly reduced by ISR photons. Fig. 10 shows that the cross-section decreases as the CM energy increases for the signal process of $e^+e^- \rightarrow A'A'\gamma$. This result suggests that it is efficient to search for signal events in low CM energy experiments for this dark photon mass.

### 4.2.2 Cross-Section Depending on Dark Photon Mass

Fig. 11 shows the cross-section dependence with respect to dark photon mass for the signal mode of $e^+e^- \rightarrow A'A'$ where each $A'$ decays into dimuon. The dark photon mass was scanned for the cross-section from 0.25 GeV to 100 GeV
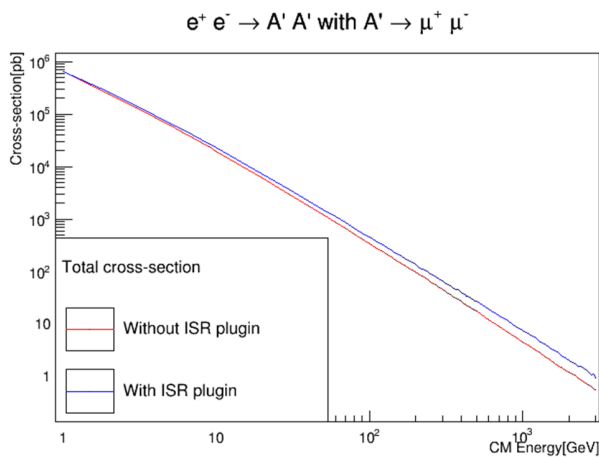
while the dark photon width was fixed at $6.7 \times 10^{-6}$ GeV. Thirteen CM energies were included, the coupling constant was fixed at 0.1, and the minimum transverse momentum ($P_T$) cut for photons and leptons was set at 0.01. Fig. 12 shows the cross-section with respect to dark photon mass for the signal process of $e^+e^- \rightarrow A'A'\gamma$ where each $A'$ decays into dimuon. The cross-section with a photon is smaller than that of it without photons. The cross-section of Belle II CM energy is larger than other future lepton colliders for dark photon mass below 5 GeV. We found the dark photon mass which produces the largest cross-section in each energy. We applied these dark photon masses to reconstruction to find maximum number of events.

### 4.2.3 Cross-Section Depending on Coupling Constant

Fig. 13 shows the cross-section dependence on coupling constant for the signal mode of $e^+e^- \rightarrow A'A'$ where each $A'$ decays into dimuon. The coupling constant was scanned for the range $10^{-5}$ to $10^{-1}$. Thirteen CM energies were included.
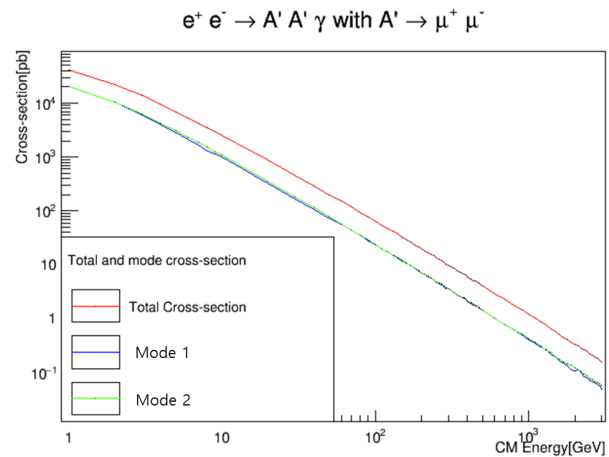


**Fig. 9.** The cross-section depending on the CM energy for $e^+e^- \rightarrow A'A'$.



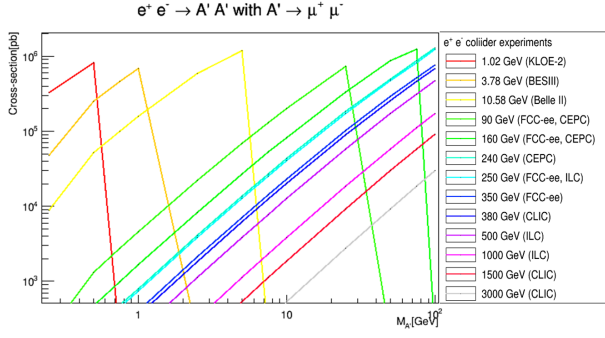**Fig. 10.** The cross-section dependending on the CM energy for $e^+e^- \rightarrow A'A'\gamma$.

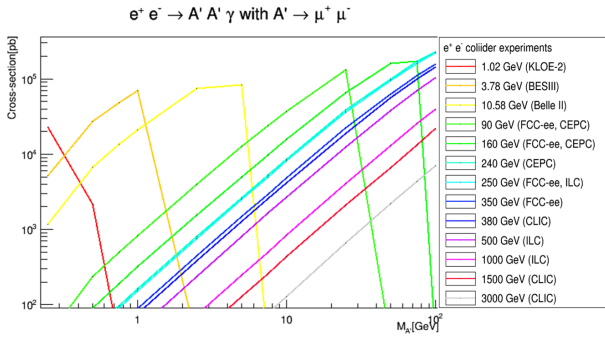**Fig. 11.** The cross-section depending on the dark photon mass ($M_{A'}$) for $e^+e^- \to A'A'$.



**Fig. 12.** The cross-section depending on the dark photon mass ($M_{A'}$) for $e^+e^- \to A'A'\gamma$.



**Fig. 13.** The cross-section depending on the coupling constant for $e^+e^- \to A'A'$.



**Fig. 14.** The cross-section depending on the coupling constant for $e^+e^- \to A'A'\gamma$.

The dark photon mass was fixed at 0.3 GeV. The dark photon decay width was fixed at $6.7 \times 10^{-6}$ GeV. The minimum transverse momentum ($P_T$) cut for photons and leptons was set at 0.01. Fig. 14 shows the cross-section according to the coupling constant for $e^+e^- \to A'A'\gamma$ where each $A'$ decays into dimuon. Overall, this cross-section is smaller than that produced without photons.

## 5. RESULTS

In order to find the best CM energy for the signal events, we studied the detector effieciency using the future circular collider (FCC-ee). Delphes was used to perform detector simulation and MadAnalysis5 was used for reconstruction on the local Linux machine. Table 5 presents detailed reconstruction parameters. Table 6 lists the CM energy, dark photon mass (width), detector pseudorapidity ($\eta$) cut, and Delphes cards for the FCC-ee. We selected deak photon mass which shows the maximum cross-section as shown in section 4.2.2.

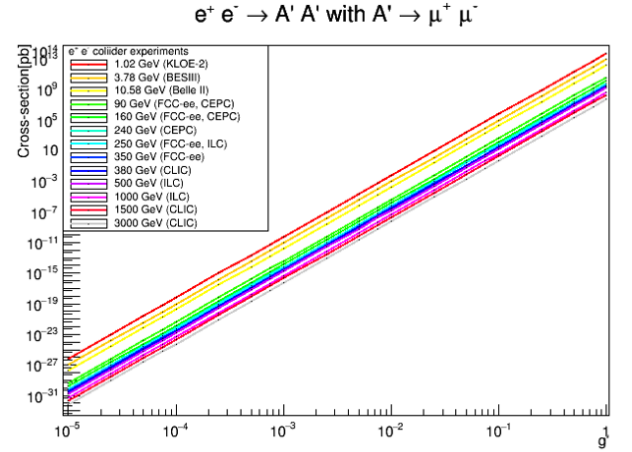Fig. 15 shows the invariant mass and transverse momentum of the $A'A'$ at FCC-ee (91 GeV) for $e^+e^- \to$

**Table 5.** Parameters of $e^+e^- \to A'A'$

| Specification | Details |
|---|---|
| Number of generated events | 1,000,000 |
| Machine | Local Linux machine |
| Simulation tool kit | Delphes, MadAnalysis5 |
| Condition | $P_{T,\mu} \geq 0.01$ GeV, $P_{T,\gamma} \geq 0.01$ GeV |

**Table 6.** Parameters of FCC-ee

| Experiments | CM energy (GeV) | Dark photon mass (width) (GeV) | Detector $\eta$ cut | Delphes card |
|---|---|---|---|---|
| FCC-ee | 91 ($e^\pm$: 45.5) | 25 ($6.7 \times 10^{-6}$) | $-3.0 \leq \eta \leq 3.0$ | Delphes_card_IDEA.tcl |
| | 160 ($e^\pm$: 80) | 75 ($6.7 \times 10^{-6}$) | | |
| | 250 ($e^\pm$: 125) | 100 ($6.7 \times 10^{-6}$) | | |
| | 350 ($e^\pm$: 175) | 100 ($6.7 \times 10^{-6}$) | | |

Adapted from Delphes (2022) with open source policy.
FCC-ee, future circular collider.

*A′A′*. It shows comparisons between generation level and reconstruction level. Fig. 16 shows the invariant mass of the *A′A′* at 160, 250, and 350 GeV, respectively. It shows comparisons between generation level and reconstruction level.

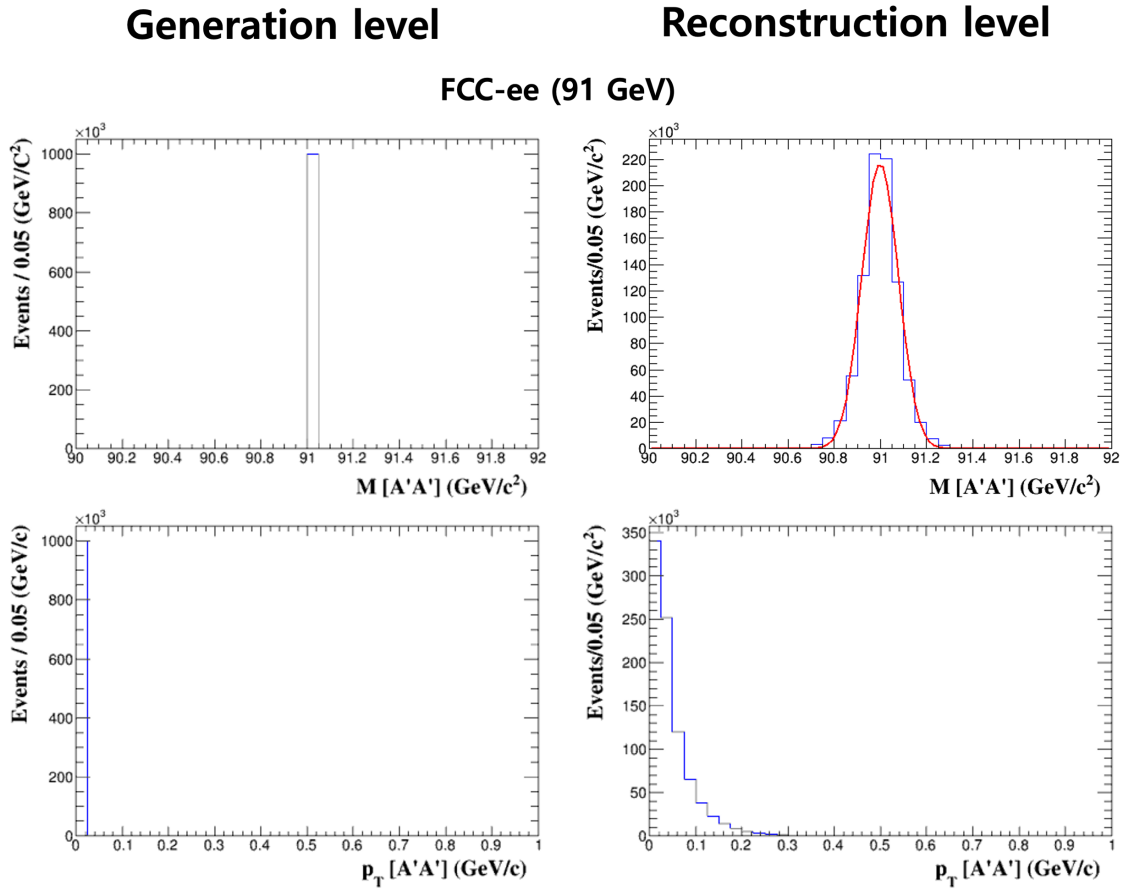We obtained the detector efficiency of each energy by

**Generation level**          **Reconstruction level**

**FCC-ee (91 GeV)**



**Fig. 15.** The invariant mass and transverse momentum of the *A′A′* at FCC-ee (91GeV). FCC-ee, future circular collider.

**Generation level**          **Reconstruction level**

**FCC-ee (160 GeV)**
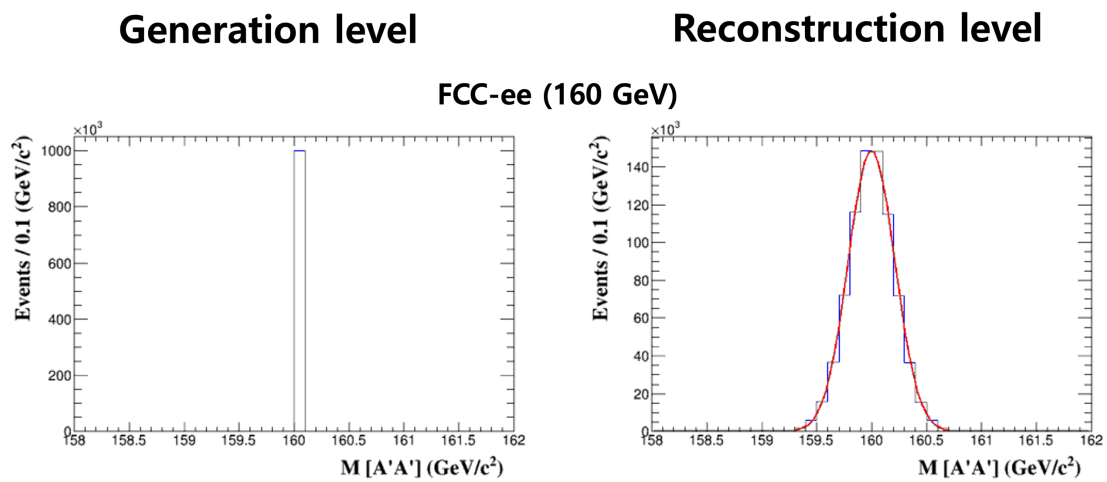


**Fig. 16.** The invariant mass of the *A′A′* at 160, 250, and 350 GeV. (Continued on the next page.)

(**Fig. 16.** Continued)
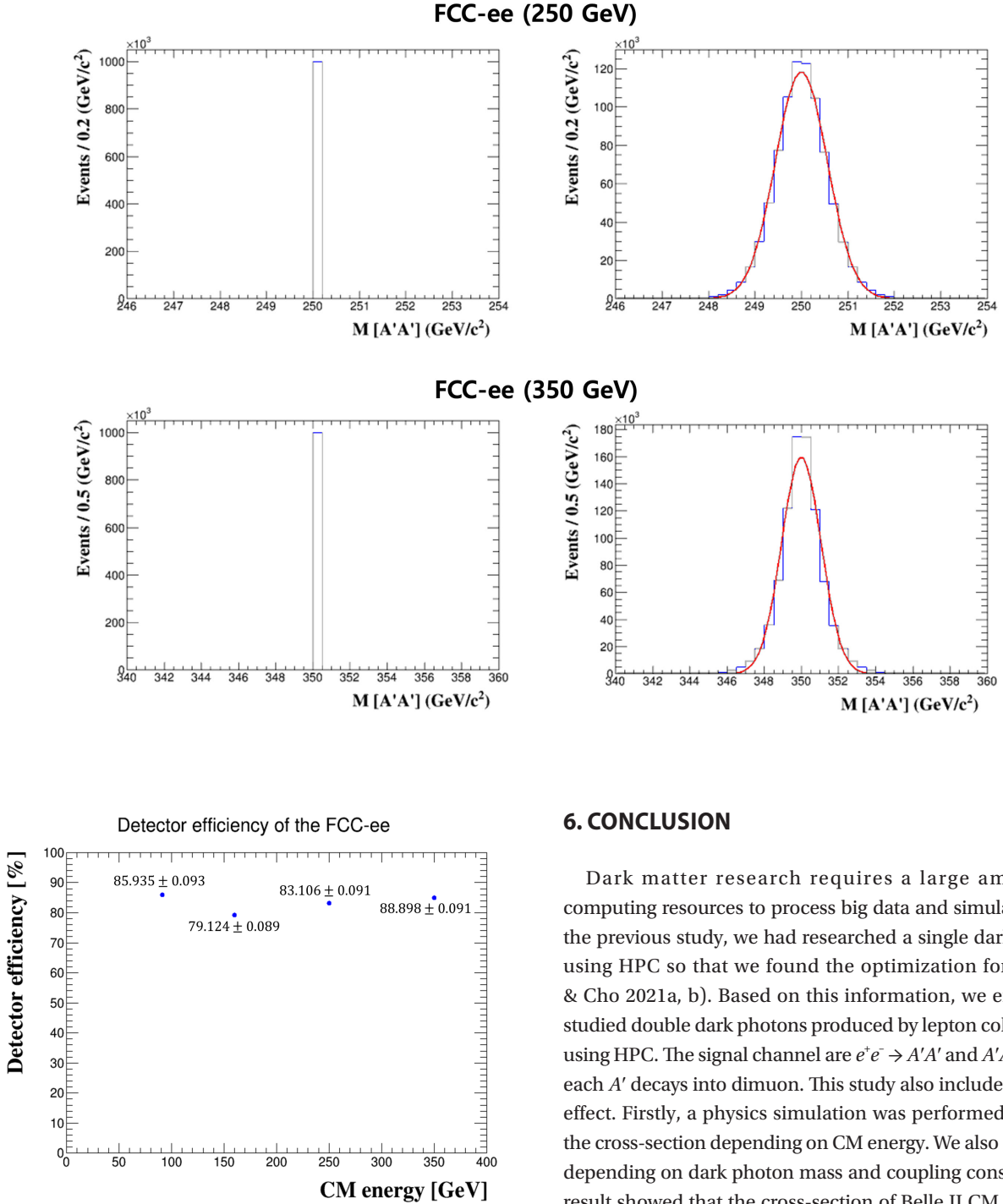
## FCC-ee (250 GeV)



## FCC-ee (350 GeV)





**Fig. 17.** Detector efficiency of FCC-ee. FCC-ee, future circular collider.

fitting the reconstructed invariant mass distribution of $A'A'$ of the reconstruction level. Fig. 17 summarize the detector efficiency results for experiments.

## 6. CONCLUSION

Dark matter research requires a large amount of computing resources to process big data and simulations. In the previous study, we had researched a single dark photon using HPC so that we found the optimization for it (Park & Cho 2021a, b). Based on this information, we effectively studied double dark photons produced by lepton colliders for using HPC. The signal channel are $e^+e^- \rightarrow A'A'$ and $A'A'\gamma$ where each $A'$ decays into dimuon. This study also included photon effect. Firstly, a physics simulation was performed to study the cross-section depending on CM energy. We also studied it depending on dark photon mass and coupling constant. The result showed that the cross-section of Belle II CM energy is larger than other future lepton colliders for dark photon mass below 5 GeV. We found dark photon mass which produces the largest cross-section in each experiment. We applied these dark photon masses to reconstruction. Finally, in order to search for double dark photons at future lepton colliders, we reported the expected number of events considering detector efficiency. The results of this study will help to explore double

dark photon events for various lepton colliders.

## ORCID

Kihong Park      https://orcid.org/0000-0003-0567-3493
Kyungho Kim      https://orcid.org/0000-0002-4659-1112
Kihyeon Cho      https://orcid.org/0000-0003-1705-7399

## REFERENCES

Alves D, Arkani-Hamed N, Arora S, Bai Y, Baumgart M, et al., Simplified models for LHC new physics searches, J. Phys. G: Nucl. Part. Phys. 39, 105005 (2012). https://doi.org/10.1088/0954-3899/39/10/105005

Alwall J, Frederix R, Frixione S, Hirschi V, Maltoni F, et al., The automated computation of tree-level and next-to-leading order differential cross sections, and their matching to parton shower simulations, J. High Energy Phys. 2014, 79 (2014). https://doi.org/10.1007/JHEP07(2014)079

Antcheva I, Ballintijn M, Bellenot B, Biskup M, Brun R, et al., Root: a C++ framework for petabyte data storage, statistical analysis and visualization, Comput. Phys. Commun. 180, 2499-2512 (2009). https://doi.org/10.1016/j.cpc.2009.08.005

Cho K, e-Science paradigm for astroparticle physics at KISTI, J. Astron. Space Sci. 33, 63-67 (2016a). https://doi.org/10.5140/JASS.2016.33.1.63

Cho K, Computational science and the search for dark matter, N. Phys.: Sae Mulli. 66, 950-956 (2016b). https://doi.org/10.3938/NPSM.66.950

Cho K, Computational science-based research on dark matter at KISTI, J. Astron. Space Sci. 34, 153-159 (2017). https://doi.org/10.5140/JASS.2017.34.2.153

Choi W, Cho K, Yeo I, Performance profiling for brachytherapy applications, Comput. Phys. Commun. 226, 180-186 (2018). https://doi.org/10.1016/j.cpc.2017.12.022

Conte E, Fuks B, Serret G, MADANALYSIS 5, a user-friendly framework for collider phenomenology, Comput. Phys. Commun. 184, 222-256 (2013). https://doi.org/10.1016/j.cpc.2012.09.009

Delphes, Git/Cards (2022) [Internet], viewed 2022 Feb 15, available from: https://cp3.irmp.ucl.ac.be/projects/delphes/browser/git/cards

Favereau J, Delaere C, Demin P, Giammanco A, Lemaître V, et al., DELPHES 3: a modular framework for fast simulation of a generic collider experiment, J. High Energy Phys. 2014, 57 (2014). https://doi.org/10.1007/JHEP02(2014)057

MadAnalysis5, Madanalysis5 (2022) [Internet], viewed 2022 Feb 18, available from: https://launchpad.net/madanalysis5

MadGraph5, Mg5amcnlo (2022) [Internet], viewed 2022 Feb 12, available from: https://launchpad.net/mg5amcnlo

Park K, Cho K, A study of dark photon at the electron-positron collider experiments using KISTI-5 supercomputer, J. Astron. Space Sci. 38, 55-63 (2021a). https://doi.org/10.5140/JASS.2021.38.1.55

Park K, Cho K, Study of dark matter at $e^+e^-$ collider using KISTI-5 supercomputer, Int. J. Contents. 17, 67-73 (2021b). https://doi.org/10.5392/IJoC.2021.17.3.067

ROOT, Analyzing petabytes of data, scientifically (2022) [Internet], viewed 2022 Feb 11, available from: https://root.cern.ch

Shuve B, Yavin I, Dark matter progenitor: light vector boson decay into sterile neutrinos, Phys. Rev. D. 89, 113004 (2014). https://doi.org/10.1103/PhysRevD.89.113004

Yeo I, Cho K, Researches on dark matter using $e^+e^-$ collider, J. Astron. Space Sci. 35, 67-74 (2018). https://doi.org/10.5140/JASS.2018.35.2.67

Yeo I, Cho K, Study on geant4 simulation toolkit using a low-energy physics profiling system, J. Korean Phys. Soc. 74, 923-929 (2019). https://doi.org/10.3938/jkps.74.923

Yeo I, Cho K, Low-energy physics profiling of the geant4 simulation tool kit on evolving computing architectures, J. Korean Phys. Soc. 76, 1047-1053 (2020). https://doi.org/10.3938/jkps.76.1047

Zyla PA, Barnett RM, Beringer J, Dahl O, Dwyer DA, et al., Review of particle physics, Prog. Theor. Exp. Phys. 2020, 083C01. https://doi.org/10.1093/ptep/ptaa104